RSC Advances

ROYAL SOCIETY OF CHEMISTRY

www.rsc.org/advances

Journal Name

RSCPublishing

ARTICLE

Synthesis and characterization of BN/Bi_2WO_6 composite photocatalysts with enhanced visible-light photocatalytic activity

Cite this: DOI: 10.1039/x0xx00000x

Received 00th January 2012,
Accepted 00th January 2012

DOI: 10.1039/x0xx00000x

www.rsc.org/

Weibin Li[a], Qi Wang[a], Liying Huang[b], Yeping Li[b], Yuanguo Xu[b], Yanhua Song[b], Qi Zhang[c], Hui Xu[a,b,*], Huaming Li[b,*]

Bi_2WO_6 modified with few-layer BN was synthesized by an impregnation method. The as-prepared products were characterized by X-ray diffraction (XRD), scanning electron microscopy (SEM), transmission electron microscopy (TEM), X-ray photoelectron spectroscopy spectra (XPS), ultraviolet-visible diffuse reflection spectroscopy (DRS) and Fourier transform infrared spectroscopy (FT-IR). The as-prepared BN/Bi_2WO_6 photocatalysts exhibited a higher photocatalytic activity for the degradation of Rhodamine B (RhB) than the pure Bi_2WO_6. The 3 wt% BN/Bi_2WO_6 photocatalyst showed the best photocatalytic activity and high stability after five runs under visible light irradiation. The enhanced visible-light photocatalytic activity could be attributed to the synergetic effect of few-layer BN and Bi_2WO_6.

Keywords: few-layer BN, Bi_2WO_6, photocatalysis, stability

Introduction

With the increase in global environmental pollution and energy crisis, green chemistry has become a necessary requirement for the sustainable development of human society. Among the variety of green chemistry techniques, semiconductor photocatalysis has been considered as a cost-effective and sustainable green chemistry technology, and it is the most promising method because it represents an easy way to complete the degradation of organic contaminants by utilizing solar energy.[1-3] The semiconductor Titanium dioxide (TiO_2) is one of the most promising semiconductor photocatalysts for the degradation of organic pollutants because of its exceptional optical and electronic properties, biological and chemical inertness, and nontoxicity.[4-7] However, the light response range and the low photocatalytic-efficiency of TiO_2 limit its applications because of its wide band gap (3.2 eV).[8] Therefore, the development of visible-light-driven photocatalysts has attracted widespread attention. Recently, lots of new photocatalysts have been performed under visible light, they typically displayed poor performance under visible light yet, because the fast recombination of photoinduced electron-hole pairs and the enhanced visible light absorption occur simultaneously.[9]

As one of the simplest Aurivillius oxides, Bismuth tungstate (Bi_2WO_6) is a promising photocatalyst due to its optical properties and excellent intrinsic physical and chemical properties, such as ferroelectric piezoelectricity, and non-linear dielectric susceptibility.[10-14] However, there are two main disadvantages existed which limit the application of pure Bi_2WO_6. Firstly, pure Bi_2WO_6 exhibits photoabsorption properties from UV light to visible light with wavelengths shorter than *ca*. 450 nm, which occupies a small percentage of the solar spectrum. Secondly, the rapid recombination of photoinduced electron-hole pairs during the photocatalytic process weakened its photocatalytic activity significantly. Recently, many efforts have been devoted to the controlled synthesis of Bi_2WO_6-semiconductor nanocomposites (such as Bi_2WO_6/TiO_2,[15] Bi_2WO_6/Ag,[16] Bi_2WO_6/C_3N_4,[17] etc.) to effectively decrease the probability of electron-hole recombination and enhance the photocatalytic activities. The hybrid composites showed higher photocatalytic activity compared with their individual single-component material. For this reason, instead of using a single semiconductor, combining two or more semiconductors with appropriate band positions to improve the photocatalytic performance is an established idea because they can lead to enhanced charge separation and interfacial charge-transfer efficiency.[18-20]

Boron nitride, especially few-layer or single-layer structure boron nitride, a structural analog of graphene, exhibits outstanding properties such as a low dielectric constant, high chemical stability, large thermal conductivity and nontoxicity. Previous reports suggest that the composites between BN and other materials showed a good performance for photocatalytic applications. For example, Huang et al.[21] successfully prepared Cu_2O octahedrons on h-BN for p-nitrophenol reduction. Wang et al.[22] prepared a high yield of boron-nitride submicron-boxes for the degradation of MO upon visible light irradiation. Fu et al.[23,24] prepared h-BN/ZnO and h-BN/TiO_2 by ball-milling. In our previous work, BN/AgBr photocatalyst was also synthesized.[25] All these composites modified with BN showed higher photocatalytic performance. This is because BN is few-layer material with a large surface. Moreover, a photocatalyst loaded on a layered or high surface area material is beneficial for reducing the rapid recombination of photogenerated electron-hole pairs that are necessary for the photocatalytic

reaction.[26,27] However, to our knowledge, no works have been published on the modification of Bi_2WO_6 with few-layer BN to improve the photocatalytic performance. Considering these advantages of Bi_2WO_6-based composite photocatalysts, we tried to combine Bi_2WO_6 with a few-layer BN to construct a stable and efficient photocatalytic system.

In this work, the composite (BN/Bi_2WO_6) was successfully prepared by impregnation method and characterized by XRD, SEM, TEM, XPS, DRS, and FT-IR. The photocatalytic activities of the as-prepared samples were evaluated by decomposition of Rhodamine B (RhB) under visible light (λ>400 nm). The results indicated that the composite showed a much higher visible-light-driven photocatalytic activity compared to the pure Bi_2WO_6.

Experimental section

2.1 Preparation of photocatalysts

2.1.1 Preparation of few-layer BN

The few-layer BN was prepared according to the method of Rao et al.[28] In a typical experimental procedure, boric acid and urea were dissolved in 40 mL de-ionized water, heated and stirred at 65 ℃. The dried mixtures were heated at 900 ℃ for 5 h in a N_2 atmosphere, then the white few-layer BN products were obtained.

2.1.2 Preparation of Bi_2WO_6

Bi_2WO_6 was prepared by hydrothermal synthesis.[29] In a typical synthesis of Bi_2WO_6, 2.435 g $Bi(NO_3)_3{\cdot}5H_2O$ and 0.8246 g $Na_2WO_4{\cdot}2H_2O$ was initially dissolved in 100 mL deionized water. After 20 minutes of ultrasonic processing, the slurry solution was centrifuged and transferred into a 25 mL Teflon-lined autoclave and subsequently heated at 160℃ for 12 h. The reactor was then allowed to cool to room temperature naturally. The precipitate was collected and washed with distilled water and ethanol, and the final products dried at 80℃ for 8 h.

2.1.3 Preparation of BN/Bi_2WO_6 photocatalysts

The BN/Bi_2WO_6 composite photocatalysts were prepared by impregnation method. For the sake of convenience, the BN/Bi_2WO_6 photocatalysts were labeled as x% BN/Bi_2WO_6 (x denotes wt% of few-layer BN in BN/Bi_2WO_6). The 1 wt% BN/Bi_2WO_6 composite photocatalysts were obtained as follows: 3 mg few-layer BN and 297 mg Bi_2WO_6 were added into 100 mL beaker, and then 15 mL ethyl alcohol was added into the above beaker. In the process of experiment, a plastic wrap was used not only to prevent the ethanol from evaporating but also to prevent dust fall into the beaker. After stirred for 11 h, the products were placed in the oven at 60 ℃ for 7 h. Similarly, the 2 wt%, 3 wt%, 5 wt% and 10 wt% composite photocatalysts were obtained, respectively.

2.2 Characterization

The crystal structure of the samples were investigated by X-ray diffraction (XRD) on a Bruker D8 diffractometer with Cu Kα radiation (λ=1.5418Å) in the range of 2θ=10-80°. The field-emission scanning electron microscopy (SEM) measurements were carried out with a field-emission scanning electron microscope (JEOL-JSM-7001F) equipped with an energy-dispersive X-ray spectroscope (EDS) operated at an acceleration voltage of 10 kV. Transmission electron microscopy (TEM) micrographs were taken with a JEOL-JEM-2010 (JEOL, Japan) operated at 200 kV. X-ray photoelectron spectroscopy (XPS) measurements were performed using a Thermo ESCALAB 250XI electron spectrometer. Ultraviolet-visible (UV-vis) diffuse reflection spectroscopy (DRS) was collected at room temperature with a UV-vis spectrophotometer (Shimadzu UV-2450, Japan) in the range of 200-800 nm, $BaSO_4$ was used as the reference. The Fourier transform infrared (FT-IR) spectra of the samples were recorded on a Nicolet Nexus 470 spectrometer.

2.3 Photocatalytic activity test

The photocatalytic activity of the BN/Bi_2WO_6 composite photocatalysts were evaluated by degrading RhB using a 300 W xenon lamp as light source with a 400 nm cutoff filter. In each experiment, 0.075 g of the composite photocatalysts were added in a Pyrex photocatalytic reactor containing 75 mL of RhB (10 mg/L) aqueous solution, and the Pyrex photocatalytic reactor was connected to a circulating water system which could keep the reaction temperature at 30 °C. Prior to irradiation, the suspension was magnetically stirred in the dark for 30 min to establish the absorption-desorption equilibrium. At given irradiation interval, 4 mL of the suspension was collected and centrifuged to remove the catalyst particles. Then the concentration of RhB was analyzed by UV-2450 spectraphotometer at a wavelength of 553 nm. By the same procedure, we also carried out the degradation of ciprofloxacin in aqueous solution.

2.4 Photoelectrochemical measurements

The photocurrents and EIS were investigated with an electrochemical analyzer (CHI660B, Chen Hua Instruments, Shanghai, China) in a standard three-electrode system, which employed a platinum wire as the counter electrode, a saturated calomel electrode (SCE) as the reference electrode and a ITO as working electrode, respectively. 5 mg sample powder was dispersed ultrasonically in a mixture of 0.5 mL ethylene glycol and 0.5 mL ethanol, and 20 μL of the resulting colloidal dispersion was drop-cast onto a piece of ITO slice with a fixed area of 0.5 cm^2 and dried in air at room temperature. A 500 W Xe arc lamp was utilized as the light source. The photocurrent measurements were performed at a constant potential of 0 V. And a 0.1 M Na_2SO_4 aqueous solution was used as the supporting electrolyte for photocurrent measurements. The samples were irradiated for several minutes until the photocurrent was stable. Then we irradiated and shielded the samples at intervals of 20 seconds to get the photocurrent analysis. Electrochemical impedance spectra (EIS) were measured at an open-circuit voltage. 5 mM $Fe(CN)_6^{3-}$/($Fe(CN)_6^{4-}$) was used as the impedance liquid.

Results and discussion

3.1 Crystal phase composition

Fig. 1 shows the XRD patterns of the as-prepared few-layer BN, Bi_2WO_6, and BN/Bi_2WO_6 composites with various BN contents. The diffraction peak at around ~25.4° can be ascribed to the (002) plane of BN (JCPDS No. 34-0421). All the diffraction peaks of BN/Bi_2WO_6 composites can be indexed to the pure orthorhombic Bi_2WO_6 (JCPDS No. 39-0256), suggesting that doping with BN didn't significantly change the structure of the Bi_2WO_6. As shown in Fig. 1, the diffraction peaks of pure Bi_2WO_6 and BN/Bi_2WO_6 composites at 28.3°, 32.8°, 47.1°, 56.0°, 58.5° and 68.8° can be attributed to the (131), (200)/(002), (202), (133), (262), and (400) crystal planes of orthorhombic Bi_2WO_6. The prepared BN and BN/Bi_2WO_6 composites have good crystallinity, but no BN phase is observed in BN/Bi_2WO_6 composites. This may be due to the low amount of BN in the composites.

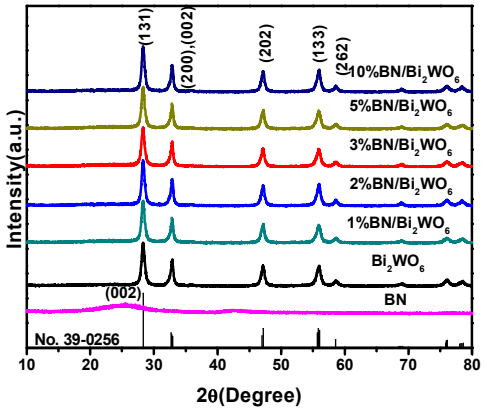

Fig. 1 XRD patterns of few-layer BN, Bi_2WO_6 and BN/Bi_2WO_6 composites

3.2 Morphology

The morphology and microstructure of samples were investigated by SEM and TEM. The pure Bi_2WO_6 was consisted of a large quantity of hierarchical sphere-like structure with the average diameter about 2~3 um (Fig. 2a). From Fig. 2b, it can be seen that Bi_2WO_6 particles are deposited on the surface of few-layer BN whom has a large surface with a thin film layer. The morphology of the 3 wt% BN/Bi_2WO_6 composite was further analyzed by TEM, from the TEM image of the 3 wt% BN/Bi_2WO_6 composite, it can be observed that Bi_2WO_6 particles locate randomly on the surface or edge of few-layer BN. The contact region between few-layer BN and Bi_2WO_6 may make great contribution to improve the separation of photo-induced electrons and holes. In addition, the EDS pattern showed that the 3 wt% BN/Bi_2WO_6 composite contains B, N, Bi, W and O element. The elements of B, N, Bi, W and O indicate that BN was successfully combined with Bi_2WO_6.

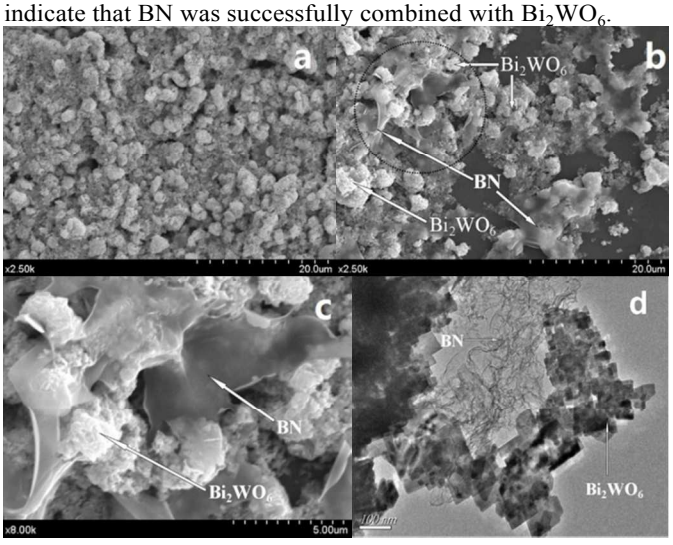

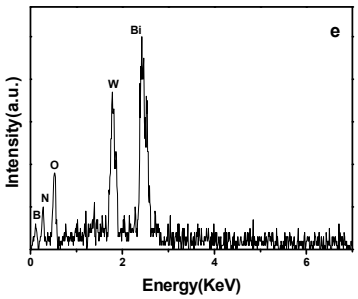

Fig. 2 (a) SEM image of Bi_2WO_6. (b) SEM image of 3 wt% BN/Bi_2WO_6. (c) Local magnified image of (b). (d) TEM image of 3 wt% BN/Bi_2WO_6. (e) EDS spectrum taken from 3 wt% BN/Bi_2WO_6.

3.3 XPS analysis

XPS was carried out to investigate the elemental composition and chemical states of the as-prepared Bi_2WO_6, few-layer BN and BN/Bi_2WO_6 composites and the results are displayed in Fig. 3. The full scan in Fig. 3a showed that Bi, O, W, B, N and C elements were present in the pure Bi_2WO_6, few-layer BN and the 3 wt% BN/Bi_2WO_6 composite (the inset of Fig. 3a shows the magnified the local area of the XPS survey spectra to distinguish the B 1s spectra). The XPS peak for C 1s is due to the adventitious hydrocarbon from the XPS instrument itself. The high-resolution spectra of Bi 4f, W 4f, O 1s, B 1s and N 1s are displayed in Fig. 3b-f, respectively. The Bi 4f region of the pure Bi_2WO_6 consists of two peaks located at 159.68 and 164.98 eV corresponding to the binding energy of Bi $4f_{7/2}$ and Bi $4f_{5/2}$, respectively, and they are consistent with the binding energies in Bi_2WO_6.[30,31] The two peaks located at 36.26 and 38.41 eV in W 4f region could be assigned to W $4f_{7/2}$ and W $4f_{5/2}$, indicating the existence of W^{6+} oxidation state. However, it is worth noting that the Bi 4f binding energy values of the 3 wt% BN/Bi_2WO_6 displayed a slight shift when compared to the pure Bi_2WO_6, the two peaks of Bi 4f shift from 159.68 eV to 159.48 eV and from 164.98 eV to 164.81 eV, and the same change was also observed in W 4f and O 1s, the two peaks of W 4f shift from 36.26 eV to 35.93 eV and from 38.41 eV to 38.08 eV. This reveals that the interaction between few-layer BN and Bi_2WO_6 results in the changes of the local environments and electron densities of the elements to some degree.[32] Fig. 3e and Fig. 3f showed the high-resolution spectra of B 1s and N 1s, respectively. The peaks of B 1s and N 1s in 3 wt% BN/Bi_2WO_6 are located in 190.64 eV and 398.01 eV, respectively, which correlated well with Ariel Ismach's[33] work about controlled synthesis of hexagonal boron nitride films. The B 1s and N 1s binding energy values of the 3 wt% BN/Bi_2WO_6 also displayed a slight shift when compared to few-layer BN, the peak of B 1s shift from 190.64 eV to 190.73 eV and N 1s shift from 398.01 eV to 398.14 eV.

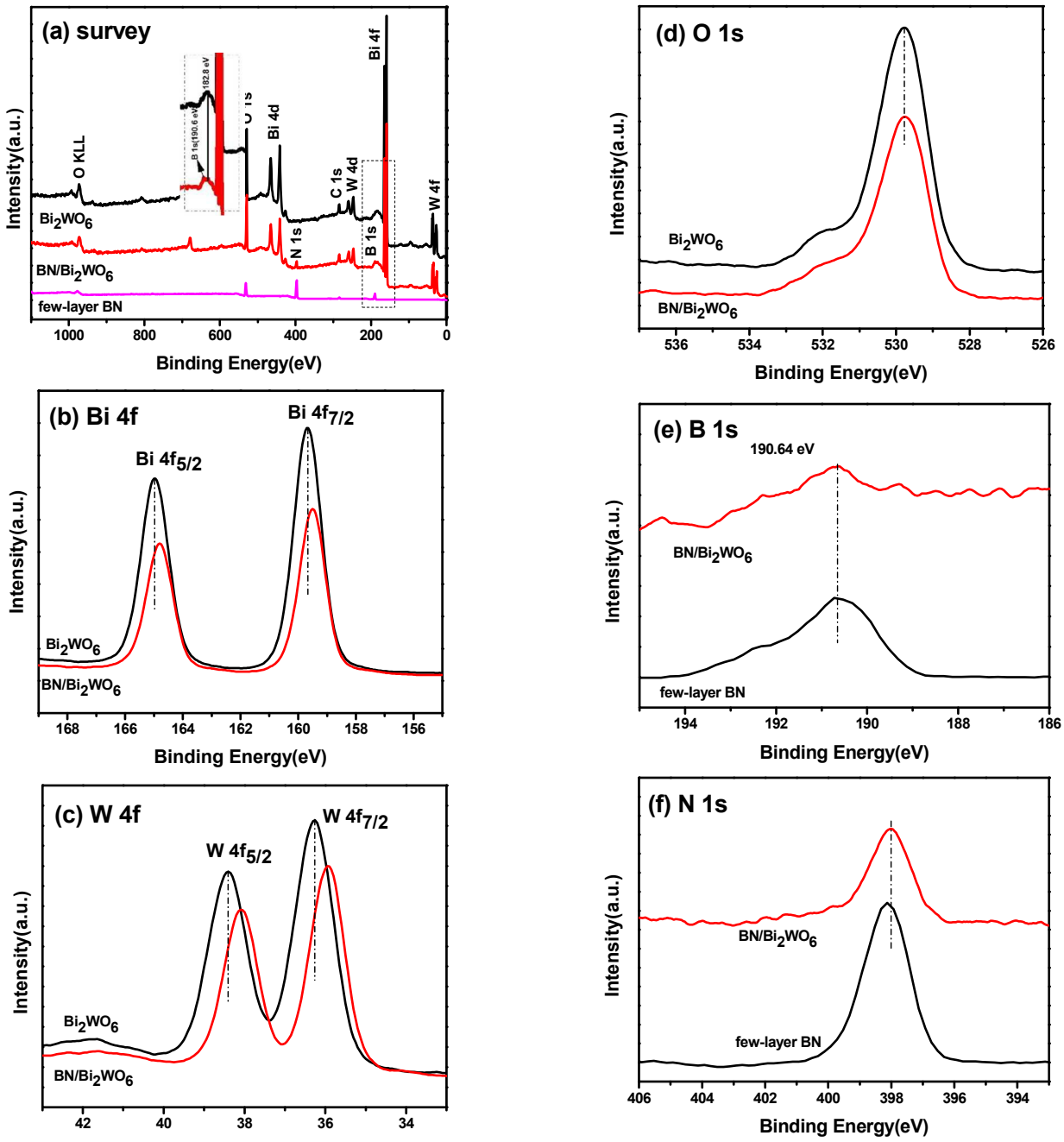

Fig. 3 (a) X-ray photoelectron survey spectra of pure Bi_2WO_6 and 3 wt% BN/Bi_2WO_6, (b) Bi 4f, (c) W 4f, (d) O 1s, (e) B 1s and (f) N 1s.

3.4 DRS analysis

Fig. 4 shows the UV-vis diffuse-reflectance spectra of the as-obtained few-layer BN, Bi_2WO_6 and BN/Bi_2WO_6 composites. The pure Bi_2WO_6 can absorb the wavelengths shorter than *ca.* 450 nm due to its intrinsic transition. After combined with few-layer BN, a slight shift of the absorption band toward the low wavelength region can be observed. This could be due to the larger band-gap BN widens the band-gap of Bi_2WO_6. The visible light absorption ability of the composites are gradually enhanced with an increase in loaded BN, (the order of the visible light absorption ability of the composites: 3 wt%>2 wt%>1 wt%) however, excessive loaded BN will decrease the visible light absorption (5 wt%, 10 wt%). The possible reasons

for that are summarized as follow: when the doping ratio is less than 3 wt%, the visible light absorption ability of the composites are gradually enhanced with an increase in loaded BN, this could be due to doping appropriate amount of BN could improve the separation efficiency of holes and electrons due to the synergetic effect between few-layer BN and Bi_2WO_6, however, excessive loaded BN will decrease the visible light absorption may due to the few-layer BN affects the light absorption of Bi_2WO_6. Fig. 4b showed the plot of $(\alpha hv)^2$ versus photon energy (hv) for the as-prepared composites and pure Bi_2WO_6, where α, h, and v are the absorption coefficient, constant, and light frequency, respectively.[34,35] The energy of the band gap is calculated by extrapolating the straight line to the abscissa axis. The band gap of the pure Bi_2WO_6 was estimated to 2.89 eV. After doping with few-layer BN, the band gap of the composites shifted to larger band gap energy.

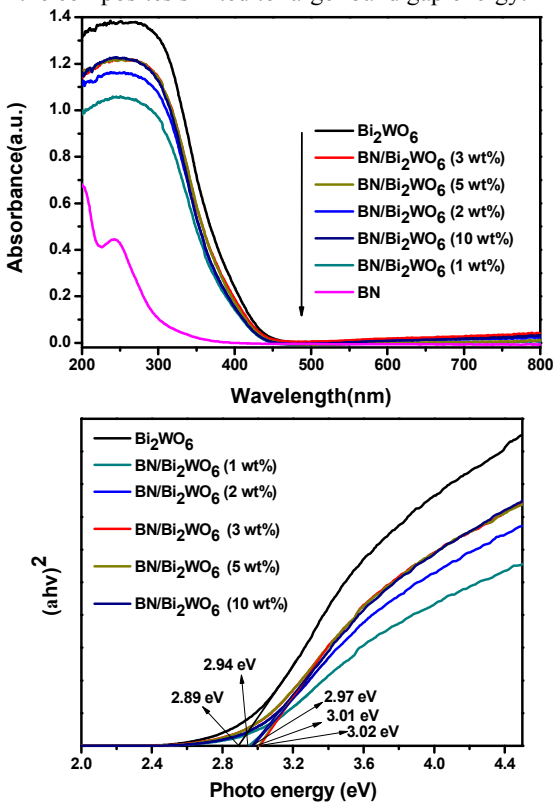

Fig. 4 (a)UV-vis diffuse reflectance spectra of BN, Bi_2WO_6, and BN/Bi_2WO_6 samples; (b) determination of the band gap energies.

3.5 FT-IR analysis

In order to further confirm the composition of the as-prepared samples, pure Bi_2WO_6, few-layer BN, and BN/Bi_2WO_6 composites were characterized by FT-IR analysis. The FT-IR spectra of the as-prepared samples are shown in Fig. 5. The main characteristic absorption bands can be observed at approximately 1378 and 805 cm^{-1} for pure BN. The former can be attributed to the stretching vibration of the B-N bond, while the latter belongs to the B-N-B out-of-plane bending vibrations.[36] For pure Bi_2WO_6, the main absorption bands at 400-800 cm^{-1} are attributed to W-O, Bi-O stretching and W-O-W bridging stretching modes.[37] These main absorption peaks are still present in BN/Bi_2WO_6 composites, also suggesting that the doping with BN didn't significantly change the structure of the Bi_2WO_6, which is consistent with the XRD result. The peak at 1378 cm^{-1} in BN/Bi_2WO_6 composites were become wider with the increase of the doping content of few-layer BN. And the two absorption bands at 1630 and 3430 cm^{-1} are assignable as the stretching and bending vibrations of the adsorbed water molecules.[38]

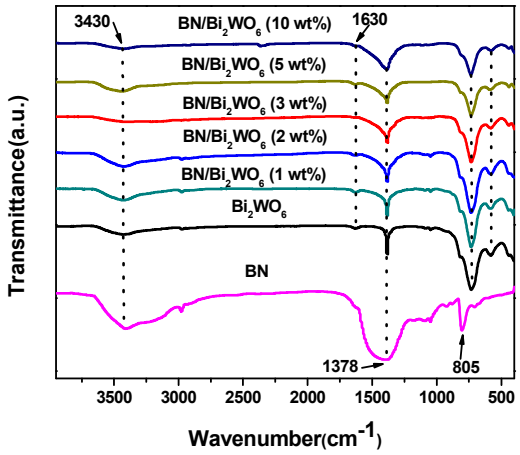

Fig. 5 FT-IR spectra of BN, Bi_2WO_6, and BN/Bi_2WO_6 samples.

3.6. Photocatalytic activity and regeneration

The photocatalytic activities of the as-prepared samples were evaluated by the degradation of Rhodamine B aqueous under visible light irradiation and the results are shown in Fig. 6, where C_0 and C_t represent the concentrations in aqueous phase at beginning and at reaction time t. All the BN/Bi_2WO_6 composites showed much higher photocatalytic activity than that of the pure Bi_2WO_6. It is obvious that the amount of BN had a great effect on the photocatalytic activity of the as-prepared samples. With the increase of the content of BN, the photocatalytic activity of the composites increased until the amount of BN reach to 3 wt%. Continue to increase the amount of BN, the photocatalytic activity of the composites decreased. So the highest photocatalytic activity reached at the proportion of BN is 3 wt%, and 98.2% of RhB was degraded after 100 min irradiation. By the same time, the rate of photocatalytic reaction was also investigated by fitting the first-order kinetic and the results were displayed in Fig. 6b and Table 1. The k value of the 3 wt% BN/Bi_2WO_6 is about 2.4 times as that of the pure Bi_2WO_6. The shift of the maximum absorption wavelength was due to N-deethylation and destruction of the conjugated structure of RhB molecule.[39] Fig. 7a showed the change in UV/vis absorption of RhB aqueous solutions under visible-light irradiation in the presence of pure Bi_2WO_6, the maximum absorption wavelength shift from 553 nm to 503 nm, which indicate that the four ethyl are not completely removed. And Fig. 7b showed the change in UV/vis absorption of RhB aqueous solutions under visible-light irradiation in the presence of 3 wt% BN/Bi_2WO_6, the maximum absorption wavelength shift from 553 nm to 497 nm, which indicate that the four ethyl are completely removed. That's to say, the degradation ability for RhB of the 3 wt% BN/Bi_2WO_6 composite is better than that of pure Bi_2WO_6. And the color of the solution changed from red to light green-yellow (the inset of Fig. 7).

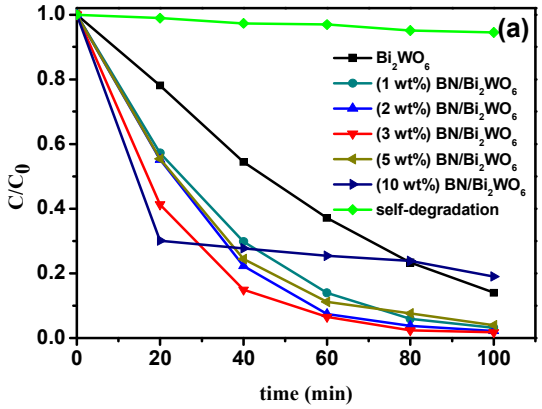

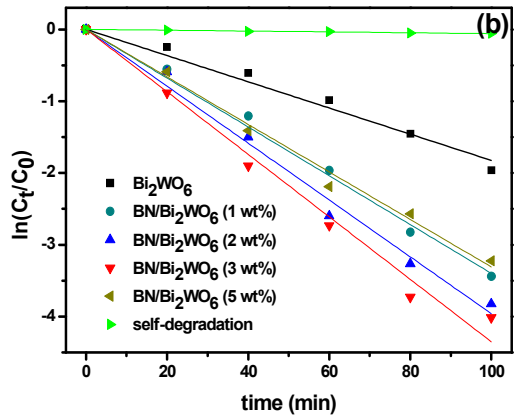

Fig. 6 (a) photocatalytic degradation of RhB by BN/Bi_2WO_6 hybrids under visible light irradiation; (b) kinetic fit diagram for RhB degradation.

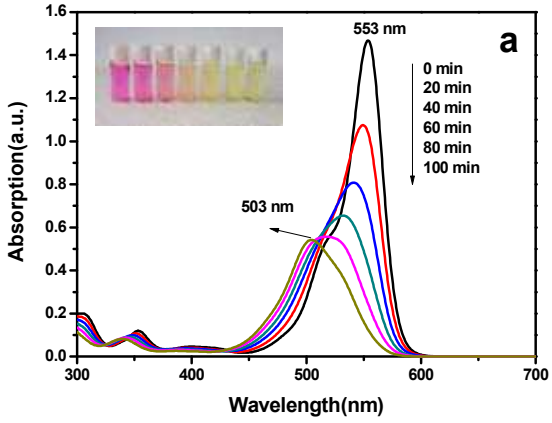

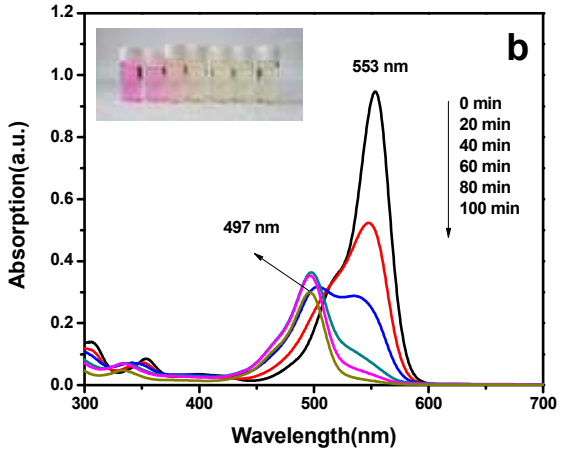

Fig. 7 Change in UV/vis absorption of RhB aqueous solutions under visible-light irradiation in the presence of (a) pure Bi_2WO_6 and; (b) 3 wt% BN/Bi_2WO_6 composite samples.

In order to investigate the generality of the photocatalytic activity for removal of other pollutants, the 3 wt% BN/Bi_2WO_6 composite was used to degrade the ciprofloxacin aqueous solution under visible light irradiation. The result in Fig. 8 showed that the ciprofloxacin conversion was 67.6% under visible light irradiation within 100 min.

Table. 1 First-order kinetic constant for RhB degradation with different photocatalysts.

Samples	$k(min^{-1})$	R^2
Bi_2WO_6	0.0183	0.9905
1 wt% BN/Bi_2WO_6	0.0340	0.9974
2 wt% BN/Bi_2WO_6	0.0396	0.9957
3 wt% BN/Bi_2WO_6	0.0435	0.9938
5 wt% BN/Bi_2WO_6	0.0331	0.9966
self-degradation	5.887E-4	0.9921

Considering the applications of photocatalysts, the regeneration of a photocatalyst is important and necessary. In our work, the 3 wt% BN/Bi_2WO_6 composite was used to investigate the stability of the photocatalyst. Before each experiment, the photocatalyst was washed by de-ionized water and ethanol, and dried at 60℃ in the oven. The results showed that BN/Bi_2WO_6 composite photocatalysts were very stable. From Fig. 9 it can be observed that there was only a slight decrease in degradation efficiency after five cycles.

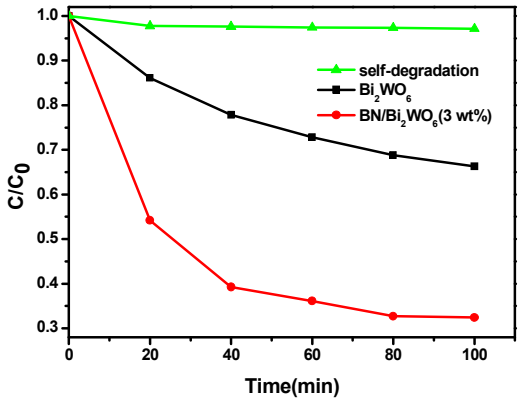

Fig. 8 Photocatalytic degradation of ciprofloxacin by Bi_2WO_6 and 3 wt% BN/Bi_2WO_6 hybrids under visible light irradiation.

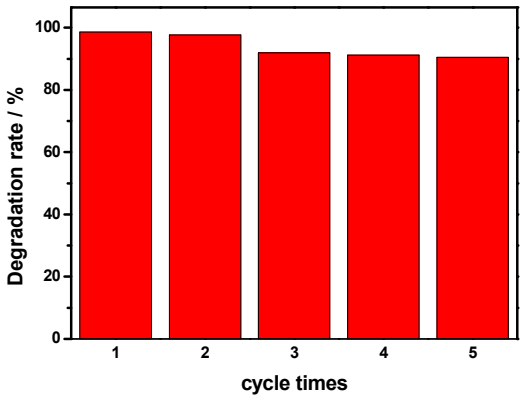

Fig. 9 Cycling runs of 3 wt% BN/Bi_2WO_6 photocatalyst for RhB degradation.

3.7. Photoelectrochemical measurements

The separation efficiency of electrons and holes may make great contribution to the photocatalytic reaction. Photocurrent produced from the photo-generated electrons in the conducting bands of semiconductor photocatalysts with leaving holes in their valence bands. Therefore, higher photocurrents are indicative of better electron and hole separation efficiencies, and thus higher photocatalytic activities.[40] The photoelectrochemical property of the pure Bi_2WO_6 and 3 wt% BN/Bi_2WO_6 composite were investigated, and the results are shown in Fig. 10. It is clear that the 3 wt% BN/Bi_2WO_6 composite exhibited a slightly higher photocurrent than the pure Bi_2WO_6 under visible light irradiation. Meanwhile, the EIS of the pure Bi_2WO_6 and the 3 wt% BN/Bi_2WO_6 composite were measured. The results are presented in Fig. 11, and the arc radius in EIS of 3 wt% BN/Bi_2WO_6 composite is smaller than the pure Bi_2WO_6. The results are in accordance with that of photocurrent, which indicate that Bi_2WO_6 modified with few-layer BN can promote the separation efficiency of electron and hole when compared to the pure Bi_2WO_6.

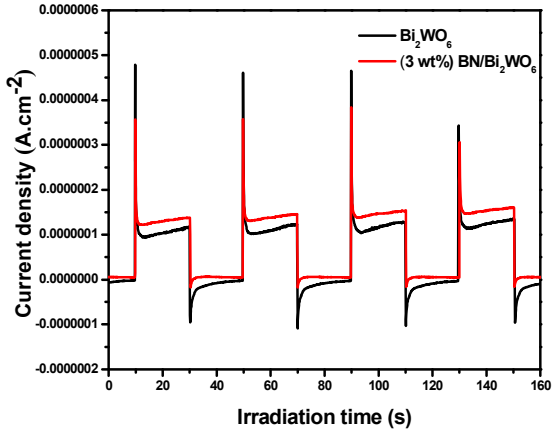

Fig. 10 Photocurrent of Bi_2WO_6 and 3 wt% BN/Bi_2WO_6 composite.

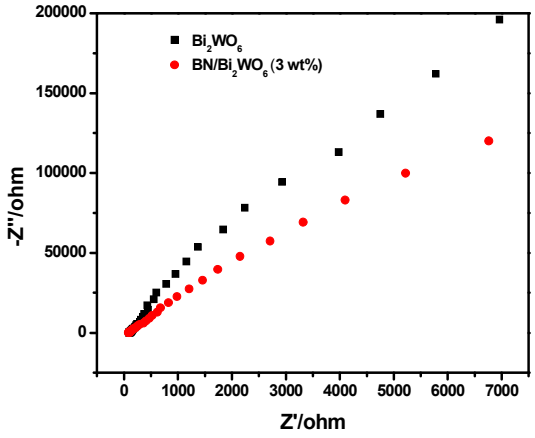

Fig. 11 The electrochemical impedance spectra of Bi_2WO_6 and 3 wt% BN/Bi_2WO_6 composite.

3.8. Possible photocatalytic mechanism

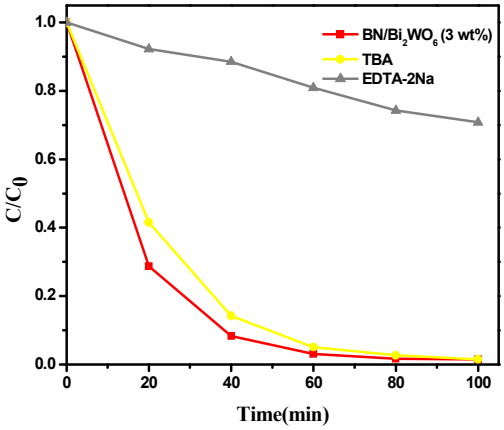

Fig. 12 Trapping experiments of active species during the photocatalytic degradation of RhB over BN/Bi_2WO_6 hybrid material under visible light irradiation.

In order to reveal the photocatalytic mechanism, it is necessary to detect the main active species in the photocatalytic process. In this work, the trapping experiments were used to determine the main active species. From the results of Fig. 12, the degradation efficiency of RhB is slightly decreased with addition of tert-butyl alcohol (a hydroxyl radical scavenger[41]), suggesting that hydroxyl radicals are not the main active species for the degradation of RhB. On the contrary, the degradation efficiency is remarkably prohibited when EDTA-2Na (hole scavenger[42]) was added. This result suggests that holes should be the main active species in the photocatalytic process.

On the basis of the above experimental results, a possible visible light photocatalytic mechanism of BN/Bi_2WO_6 composite photocatalyst is proposed in Fig. 13. Under visible light irradiation, Bi_2WO_6 is excited and the corresponding photoinduced electrons and holes are generated. The photoinduced electrons can be excited from the VB to the CB of Bi_2WO_6 and transfered to the surface of few-layer BN, leaving the holes to the VB of Bi_2WO_6. The high surface area of BN made it easier to transfer the photoinduced electrons, which promote the separation efficiency of photoinduced electron-hole pair and thus an enhanced photocatalytic activity. It is consist with the results of the photocurrent and EIS analysis.

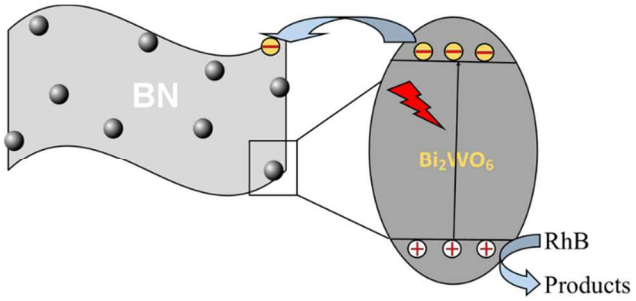

Fig. 13 Schematic of the separation and transfer of photogenerated charges in the BN/Bi_2WO_6 composite photocatalyst combined with the possible reaction mechanism of photocatalytic procedure.

Conclusions

In summary, we have successfully prepared the BN/Bi_2WO_6 composite via impregnation method. The hybrid material showed an enhancement of photocatalytic efficiency and high stability than pure Bi_2WO_6 under visible light irradiation. The doping amount of BN have an obvious effect on the photocatalytic activity, and the optimal doping amount reached at 3 wt%, which 98.2% of RhB was degraded after 100 min irradiation. The high photocatalytic activity of the BN/Bi_2WO_6 composites could be attributed to the synergetic effect of few-layer BN and Bi_2WO_6.

Acknowledgements

This work was supported by the National Nature Science Foundation of China (21476097, 21407065, 21406094), Natural Science Foundation of Jiangsu Province (BK20131207 and BK20140533), Postdoctoral Foundation of China (2014M551520 and 2013M541619) and A Project Funded by the Priority Academic Program Development of Jiangsu Higher Education Institutions.

Notes and references

[a] *School of Environment, Jiangsu University, Zhenjiang 212013, P. R. China*
[b] *Institute for Energy Research, Jiangsu University, Zhenjiang 212013, P. R. China*
[c] *Hainan Provincial Key Lab of Fine Chemistry, Hainan University, Haikou, Hainan 570228, P.R. China*
Corresponding author: *Tel.:+86-0511- 88791800; Fax: +86-0511-88791708*
E-mail address: xh@ujs.edu.cn; lihm@ujs.edu.cn

1 H. Tong, S. Ouyang, Y. Bi, N. Umezawa, M. Oshikiri and J. Ye, *Adv. Mater.*, 2012, **24**, 229-251.
2 R. Asahi, T. Morikawa, T. Ohwaki, K. Aoki and Y. Taga, *Science*, 2001, **293**, 269-272.
3 Y. Peng, S.C. Qin, W.S. Wang and A.W. Xu, *CrystEngComm*, 2013, **15**, 6518-6525.
4 A.L. Linsebigler, G.Q. Lu, J.T. Yates, *Chem. Rev*. 1995, **95**, 735-758.
5 X.B. Chen, S.S. Mao, *Chem. Rev*. 2007, **107**, 2891-2959.
6 X.Y. Pan, M.Q. Yang, X.Z. Fu, N. Zhang, Y.J. Xu, *Nanoscale* 2013, **5**, 3601-3614.
7 Y. Zhang, Z.R. Tang, X. Fu, Y.J. Xu, *ACS Nano* 2010, **4**, 7303-7311.
8 L. Ge, M.X. Xu, H.B. Fang, *Appl. Surf. Sci*. 2006, **253**, 720-725.
9 X. Zhang, K. Udawa, Z. Liu, S. Nishimoto, C. Xu, Y. Lu, H. Sakai, M. Ave, T. Marakoi and A. Kujishima, *J. Photochem. Photobiol. A*, 2009, **202**, 39-47.
10 J. Ren, W. Wang, L. Zhang, *Catal. Commun.* 2009, **10**, 1940-1943.
11 Y. Shi, S. Feng, C. Cao, *Mater. Lett.* 2000, **44**, 215-218.
12 C. Zhang, Y. Zhu, *Chem. Mater.* 2005, **17**, 3537-3545.
13 L. Wu, J. Bi, Z. Li, X. Wang, X. Fu, *Catal. Today* 2008, **131**, 15-20.
14 M. Shang, W. Wang, H. Xu, *Cryst. Growth Des*. 2009, **9**, 991-996.
15 M. Shang, W. Wang, S. Sun, L. Zhou, L. Zhang, *J. Phys. Chem. C* 2008, **112**, 10407-10411.
16 J. Ren, W. Wang, S. Sun, L. Zhang, J. Chang, *Appl. Catal., B: Environmental* 2009, **92**, 50-55.
17 Y. Wang, X. Bai, C. Pan, J. He, Y. Zhu, *J. Mater. Chem.* 2012, **22**, 11568-11573.
18 X. Wang, Q. Xu, M. R. Li, S. Shen, X. L. Wang, Y. C. Wang, Z. C. Feng, J. Y. Shi, H. X. Han and C. Li, *Angew. Chem. Int. Ed*., 2012, **51**, 13089-13092.9.
19 T. Kawahara, Y. Konishi, H. Tada, N. Tohge, J. Nishii and S. Ito, *Angew. Chem. Int. Ed*., 2002, **41**, 2811-2813.
20 X. Wang, S. Shen, S. Q. Jin, J. X. Yang, M. R. Li, X. L. Wang, H. X. Han and C. Li, *Phys. Chem. Chem. Phys*., 2013, **15**, 19380-19386.
21 C.J. Huang, W.Q. Ye, Q.W. Liu, X.Q. Qiu, *ACS Appl. Mater. Interfaces,* 2014, **6(16)**, 14469-14476.
22 M. Wang, M.H. Li, L.Q. Xu, L.C. Wang, Z.C. Ju, G.D. Li, Y.T. Qian, *Catal. Sci. Technol*. 2011, **1**, 1159-1165.
23 X.L. Fu, Y.F. Hu, T. Zhang, S.F. Chen, *Appl. Surf. Sci.* 2013, **280**, 828-35.
24 X.L. Fu, Y.F. Hu, Y.G. Yang, W. Liu, S.F. Chen, *J. Hazard. Mater.* 2013, **244**, 102-10.
25 J.J. Chen, J.X. Zhu, Z.L. Da, H. Xu, J. Yan, H.Y. Ji, et al. *Appl. Surf. Sci.* 2014, **313**, 1-9.
26 E. Dvininov, M. Ignat, P. Barvinschi, M.A. Smithers, E. Popovici, *J. Hazard. Mater*. 2010, **177**, 150-158.
27 M. Shang, W.Z. Wang, L. Zhang, *J. Hazard. Mater*. 2009, **167**, 803-809.
28 A. Nag, K. Raidongia, K.P.S.S. Hembram, R. Datta, U.V. Waghmare, C.N.R. Rao, *ACS Nano* 2010, **4**, 1539-1544.
29 C. Zhang and Y.F. Zhu*, *Chem. Mater.* 2005, **17**, 3537-3545.
30 M. Ge, Y. Li, L. Liu, Z. Zhou, W. Chen, *J. Phys. Chem. C* 2011, **115**, 5220-5225.
31 Y. Fu, C. Chang, P. Chen, X. Chu, L. Zhu, *J. Hazard. Mater*. 2013, **254-255**, 185-192.
32 Y Peng, M Yan, Q.G. Chen, C.M. Fan, H.Y. Zhou and A.W. Xu*, *J. Mater. Chem. A*, 2014, 2, 8517-8524.
33 A. Ismach, H. Chou, D.A. Ferrer, Y. Wu, S. Mcdonnell, H.C. Floresca, A. Covacevich, C. Pope, R. Piner, M.J. Kim, *ACS Nano* 2012, **6**, 6378-6385.
34 G. Cheng*, F.F. Xu, Florian J. Stadler, and R. Chen*, *RSC Adv.*, 2015, **5**, 64293-64298.
35 G. Cheng, Florian J. Stadler, *J. Colloid Interface Sci.*, 2015, **438**: 169-178.
36 R. Geick, C.H. Perry, G. Rupprecht, *Phys. Rev*. 1966, **146**, 543-547.

37 J. Yu, J. Xiong, B. Cheng, Y. Yu, J. Wang, *J. Solid State Chem*. 2005, **178**, 1968-1972.
38 Z. Chen, B. Lin, B. Xu, X. Li, Q. Wang, K. Zhang, M. Zhu, *J. Porous Mater*. 2011, **18**, 185-193.
39 T.X. Wu, G.M. Liu, J.C. Zhao, H. Hidaka, N. Serpone, *J. Phys. Chem. B* 1998, **102**, 5845-5851.
40 Q.J. Xiang, J.G. Yu, M. Jaroniec, *J. Phys. Chem. C* 2011, **115**, 7355-7363.
41 C. Minero, G. Mariella, V. Maurino, D. Vione, E. Pelizzetti, *Langmuir* 2000, **16**, 8964-8972.
42 J.H. Zhou, C.Y. Deng, S.H. Si, Y. Shi, X.L. Zhao, *Electrochim. Acta* 2011, **56**, 2062-2067.